Heliyon 8 (2022) e09919

Contents lists available at ScienceDirect

Heliyon

journal homepage: www.cell.com/heliyon

Research article

Immobilization of laccase on chitosan functionalized halloysite nanotubes for degradation of Bisphenol A in aqueous solution: degradation mechanism and mineralization pathway

Zhaobo Wang [a,b], Dajun Ren [a,b,*], Yaohui Cheng [a,b], Xiaoqing Zhang [a,b], Shuqin Zhang [a,b], Wangsheng Chen [a,b]

[a] College of Resource and Environmental Engineering, Wuhan University of Science and Technology, Wuhan 430081, China
[b] Hubei Key Laboratory for Efficient Utilization and Agglomeration of Metallurgic Mineral Resources, Wuhan University of Science and Technology, Wuhan, Hubei 430081, China

GRAPHICAL ABSTRACT

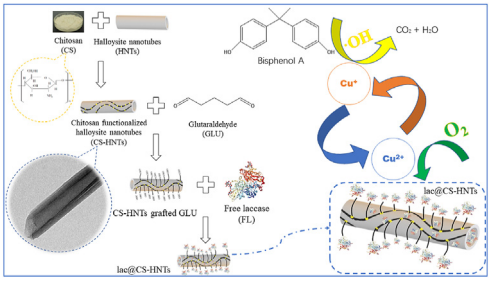

ARTICLE INFO

Keywords:
EDCs
BPA
Laccase
Chitosan
Halloysite nanotubes

ABSTRACT

As a hazardous organic chemical raw material, Bisphenol A (BPA) has attracted a great deal of scientific and public attention. In this study, the chitosan functionalized halloysite nanotubes immobilized laccase (lac@CS-HNTs) was prepared by simultaneous adsorption-covalent binding method to remove BPA for the first time. We optimized the preparation of lac@CS-NHTs by controlling one-factor variable method and response surface methodology (RSM). The cubic polynomial regression model via Design-Expert 12 was developed to describe the optimal preparation conditions of immobilized laccase. Under the optimal conditions, lac@CS-NHTs obtained the maximum enzyme activity, and the enzyme loading was as high as 60.10 mg/g. The results of batch removal experiment of BPA showed that under the optimum treatment condition, the BPA removal rate of lac@CS-NHTs, FL and heat-inactivated lac@CS-NHTs was 87.31 %, 60.89 % and 24.54 %, respectively, which indicated that the contribution of biodegradation was greater than adsorption. In addition, the relative activity of lac@CS-NHTs dropped to about 44.24 % after 8 cycles of BPA removal, which demonstrated that lac@CS-NHTs have the potential to reduce costs in practical applications. Finally, the possible degradation mechanism and mineralization pathway of BPA were given via High-performance liquid chromatography (HPLC) analysis and gas chromatography-mass spectrometry (GC-MS) analysis.

* Corresponding author.
E-mail address: dj_ren@163.com (D. Ren).

https://doi.org/10.1016/j.heliyon.2022.e09919
Received 9 March 2022; Received in revised form 19 April 2022; Accepted 6 July 2022

1. Introduction

Endocrine disrupting chemicals (EDCs) are defined as an exogenous chemical that interferes with the endocrine system, also known as environmental hormones. EDCs interfere with hormones that maintain homeostasis, thereby affecting the normal development and reproduction of organisms [1]. Bisphenol A (BPA) is an important organic chemical raw material, which is mainly used in the production of polycarbonates and epoxy resins, and is also one of the typical EDCs [2]. BPA can enter the food chain through the living environment of food-producing organisms, be released from food contact materials [3]. Traditionally, BPA has been considered a weak estrogen [4], it can interfere with endocrine signaling pathways at low doses in organisms [5, 6]. Hence, for decades, BPA has attracted a great deal of scientific and public attention [7].

In the existing research, the common methods of removing BPA are mainly divided into physical adsorption [8], chemical oxidation [9] and biodegradation [10]. Compared with the traditional physical and chemical methods [11, 12], which present a high cost and lead to the formation of hazardous by-products, the biodegradation has been considered as a possible alternative [13]. In addition, bio-enzyme present several advantages such as high catalytic efficiency, high substrate specificity, no toxicity and mild reaction conditions in biodegradation method [14]. The common bio-enzymes for BPA removal include horseradish peroxidase [15], tyrosinase [16] and multiple ligninolytic enzymes (like lignin peroxidases, manganese peroxidase and laccase) [17, 18, 19].Compared to H_2O_2 requirement of fungal peroxidases, the unique feature of laccase is that molecular oxygen can be used as the sole electron acceptor to catalyze the oxidation of BPA [20]. Liu et al. [21] verified the catalytic degradation of BPA by laccase, the results showed that the degradation rate of BPA reached 97.68 % after 1 h reaction (44.6 °C, 5 mg/L BPA concentration, pH 5.20). Unfortunately, the activity of free laccase is susceptible to interference by environmental factors (temperature, pH, ionic strength, etc.), thus limiting its application in wastewater treatment [22].

Thus, the immobilization technology of laccase was developed to enhance the tolerance and stability of laccase to environmental conditions and obtain the ability to reuse [23]. Traditional immobilization techniques include cross-linking, adsorption, covalent bonding [24] and entrapment/encapsulation [25]. In previous research [26], we optimized the preparation of alkali-modified immobilized laccases (lac@A-MB) under adsorption method, adsorption-crosslinking method and covalent bonding method. The results showed that stability of lac@A-MB was compared with other literatures [27, 28, 29], which provided a basis for the practical application of different methods for immobilizing laccase. Among the reported immobilization methods, the unique hollow tubular structure, negatively charged surface, high specific surface area, and good biocompatibility of chitosan functionalized halloysite nanotubes (CS-HNTs) make them promising laccase immobilization carriers [30, 31, 32, 33, 34]. However, these methods focus too much on the covalent binding of laccase and ignore the excellent adsorption properties of laccase on the inner and outer surfaces of the material. Therefore, a novel immobilization strategy is proposed in this paper, in which laccases are immobilized on CS-NHTs by a simultaneous adsorption-covalent binding method. In addition, this method was also particularly suitable for BPA removal from aqueous solutions. To the best of our knowledge, prior to this study, there has been no report on the removal of BPA by CS-NHTs immobilized laccase (lac@CS-NHTs).

2. Materials and methods

2.1. Chemicals

Bovine serum albumin (BSA), NaOH, phosphoric acid, Coomassie brilliant blue G-250, Chitosan (CS), glutaraldehyde (GLU) and bisphenol A (BPA) were purchased from Sinopharm Group Chemical Reagent Co., Ltd (analytical grade). Halloysite nanotubes (HNTs, 99.96 %) were purchased from Xi'an Mingchuangda Biotechnology Co., Ltd. Laccase (0.99 U/mg) from *Trametes versicolor* and (3-ethylbenzothiazoline-6-sulfonate) diammonium salt (ABTS, $\geq$ 98%) were purchased from Sigma-Aldrich.

2.2. Characterization

The Scanning electron microscope (SEM) and Transmission electron microscope (TEM) studies were carried out in a Zeiss Sigma 300 and a FEI TF20, respectively. The nitrogen adsorption-desorption isotherm (BET) was measured on the ASAP 2460 surface area and porosity analyzer. Thermal gravimetric analyses (TGA) was performed on a TGA 5500 thermoanalyzer, the sample was heated in a continuous-flow of N_2 from 25 up to 800 °C with 10 °C/min. X-ray diffraction (XRD) analysis was performed by Bruker D8A X-ray diffractometer using Cu-Kα radiation (tube voltage: 40 kV; current: 40 mA; scan angle 2θ range: 10–80°; scan rate: 5°/min. Fourier transform infrared spectroscopy (FT-IR) was performed on a Thermo Scientific Nicolet 6700 Fourier transform infrared spectrometer, and the scanning range was 4000 cm^{-1}–400 cm^{-1}.

2.3. Preparation optimization of CS-HNTs and lac@CS-HNTs

Chitosan (CS) solution (0.5 g CS in 2 % acetic acid solution) and halloysite nanotubes (HNTs) suspension (1 g HNTs in 50 mL deionized water) were mixed together at 25 °C for 24 h (300 rpm). The mixture was then filtered, washed with distilled water, dried at 60 °C, the obtained solid was Chitosan functionalized halloysite nanotubes (CS-HNTs).

Chitosan functionalized halloysite nanotubes immobilized laccase (lac@CS-HNTs) was prepared by simultaneous adsorption-covalent binding method. For this purpose, 0.1 g CS-HNTs were added into 20 mL 0.6 % glutaraldehyde (GLU) solution and stirred at 25 °C for 2 h firstly. Then, the obtained mixture was centrifuged at 4000 rpm for 10 min, washed with acetic acid-sodium acetate buffer solution (0.1 M, pH 5), dried at 60 °C, the obtained solid was CS-HNTs grafted GLU. At last, the prepared material and 10 mL free laccase (FL) solution were mixed together for a certain time (300 rpm). In this process, the aldehyde groups at both ends of GLU can react with the amino groups in both CS and FL to form Schiff bases (SB). The mixture was then filtered, washed with acetic acid-sodium acetate buffer solution (0.1 M, pH 5), the obtained sample was lac@CS-HNTs. Figure 1 showed the preparation process of chitosan functionalized halloysite nanotubes (CS-HNTs) and chitosan functionalized halloysite nanotubes immobilized laccase (lac@CS-HNTs). The preparation process of lac@CS-HNTs was optimized by controlling one-factor variables, the variables were laccase dosage (0.1–2.0 mg/mL), laccase solution pH (3–9) and reaction time (0.5–6.0 h); the dependent variables were relative enzyme activity (RA, %) and enzyme loading (E, mg/g) of immobilized laccase. The above experiment was repeated 3 times to ensure the reliability of the data. In order to further optimize the preparation conditions of lac@CS-HNTs, based on the single factor experimental data, this study used the Design-Expert 12 (Stat-Ease, Inc, Minneapolis, MN 55413, USA) to design experiments via the response surface methodology (RSM) [35]. Box Behnken Design (BBD) as one of the commonly used RSM, it was usually employed to evaluate the interaction between the independent experimental factors and the observed responses [36]. In this work, the 3-factor Box-Behnken design were used to optimize the immobilization conditions of laccase, where laccase dosage (A), laccase solution pH (B) and reaction time (C) are the 3 independent factors selected for the RA of immobilized laccase (Y) as design response (Table S1 and Table S2 in the supplementary material showed the experimental range and level of the independent variable and the Box-Behnken experimental design in the supplementary material).

2.4. Determination of enzyme activity and enzyme loading

The laccase activity was determined via ABTS method. The absorbance of reaction mixture at 420 nm was measured via ultraviolet-visible

(UV-Vis) spectrophotometer [37]. Units of enzyme activity (U) are defined as the amount of enzyme required to consume 1 μmol of substrate in 1 min [38]. The calculation formula of specific activity (SA, U/mg) and relative activity (RA, %) are as follows (Eqs. (1) and (2)):

$$SA = \frac{A}{m} \tag{1}$$

$$RA = \frac{A}{A_{max}} \times 100\ \% \tag{2}$$

where A (U) is laccase activity, and m (mg) is the mass of laccase; A_{max} (U) is the maximum enzyme activity.

The laccase concentration in the enzymatic extracts was determined by the Bradford method. The correlation coefficient R^2 was 0.998, and the fitting curve was y = 0.1061 x + 0.4012 (Figure S1 in the supplementary material). The formula of enzyme loading (E, mg/g) was as follows (Eq. (3)):

$$E = \frac{m_0 - m_1}{M} \tag{3}$$

where m_0 is the enzyme dosage (mg), m_1 is the enzyme content in supernatant (mg), and the M is total weight of immobilized laccase (g).

2.5. Stability of free laccase and lac@CS-NHTs

The thermostability of free laccase and lac@CS-NHTs was determined by immersing them in the temperatures range of 30–75 °C. The thermal tolerance of free laccase and lac@CS-NHTs was determined by immersing them in pure water at 50 °C for 2 h. The pH stability of free laccase and lac@CS-NHTs was determined in acetic acid-sodium acetate buffer solution for 2 h in the pH range 3.0–11.0. The storage stability was determined by measuring the RA of free laccase and lac@CS-NHTs in acetic acid-sodium acetate buffer solution (0.1 M, pH 5) within 30 d. The above experiment was repeated 3 times to ensure the reliability of the data.

2.6. The batch removal experiment of BPA

100 mg of lac@CS-NHTs, 100 mg of thermally inactivated lac@CS-NHTs (to exclude the effect of adsorption) and same equivalent FL were added in 250-mL Erlenmeyer flasks containing 100 mL of BPA solution. The flasks were incubated on an orbital shaker (300 rpm) and in complete darkness to avoid BPA photodegradation. The above batch degradation experiment of BPA was conducted by controlling one-factor variables, the variables were initial BPA solution pH (3–9), initial BPA solution concentration (2–50 mg/L), reaction time (0.5–12.0 h) and temperature (25–55 °C); the dependent variables was degradation rate (W) or removal rate (R). The degradation rate (W) and removal rate (R) are calculated as follows (Eqs. (4) and (5)):

$$W = \frac{C_0 - C_e}{C_0} \times 100\% \tag{4}$$

$$R = \frac{C_0 - C_e}{C_0} \times 100\% \tag{5}$$

where C_0 is the initial BPA concentration (mg/L), C_e is the final BPA concentration (mg/L).

BPA was measured by high performance liquid chromatography (HPLC, UltiMate 3000, DIONEX) under Thermo SCIENTIFIC C18 reverse phase column (250 mm × 4.6 mm I.D., 5 μm). The peak area showed a good linear relationship with the concentration of BPA, the correlation coefficient R^2 was 0.9991, and the fitting curve was y = 0.1288x-0.3732 (Figure S1b in the supplementary material). In order to further study the degradation mechanism and pathway of BPA by lac@CS-HNTs, the Agilent 7890B gas chromatography-mass (GC-MS) spectrometer (USA) was used to detect the degradation products of BPA.

3. Results and discussion

3.1. Characterization analysis

The structural morphologies of HNTs (Figure 2a), CS-HNTs (Figure 2b) and lac@CS-HNTs (Figure 2c) were observed by SEM analysis. The SEM images showed that the tubular form of HNTs was clearly visible and the structure was compact. Although, the grafting of CS and HNTs is not visible in Figure 2b and c, the tubular form and lumen of CS-HNTs could observed in the image, and the CS-HNTs showed a wider tubular morphology. These observations indicated that CS was loaded on the surface of CNTs and did not destroy the structure of HNTs. The TEM analysis of HNTs (Figure 2d), CTS-HNTs

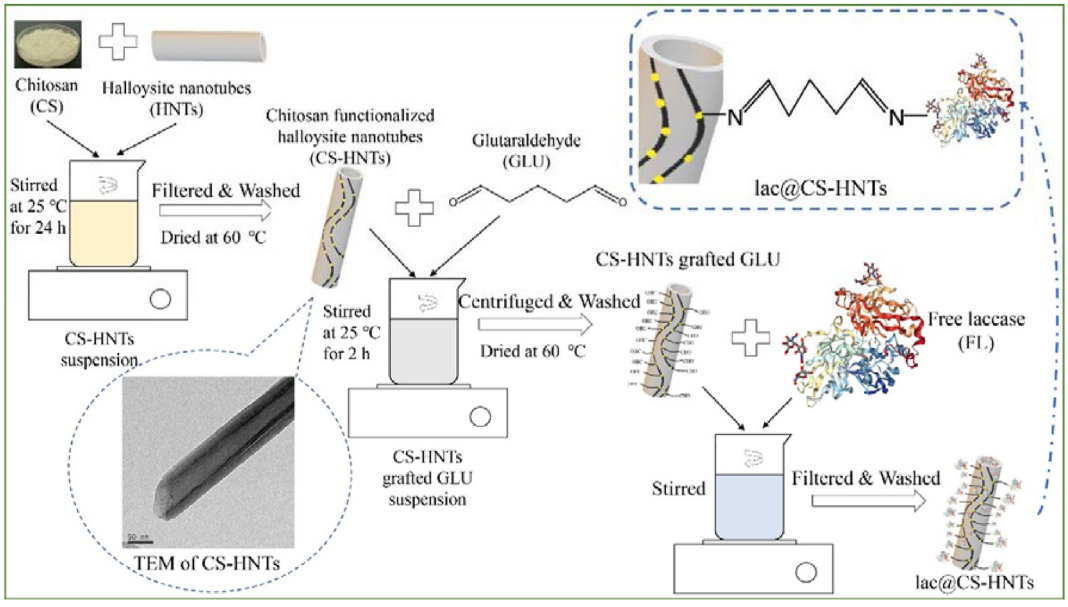

Figure 1. The preparation process of chitosan functionalized halloysite nanotubes (CS-HNTs) and chitosan functionalized halloysite nanotubes immobilized laccase (lac@CS-HNTs).

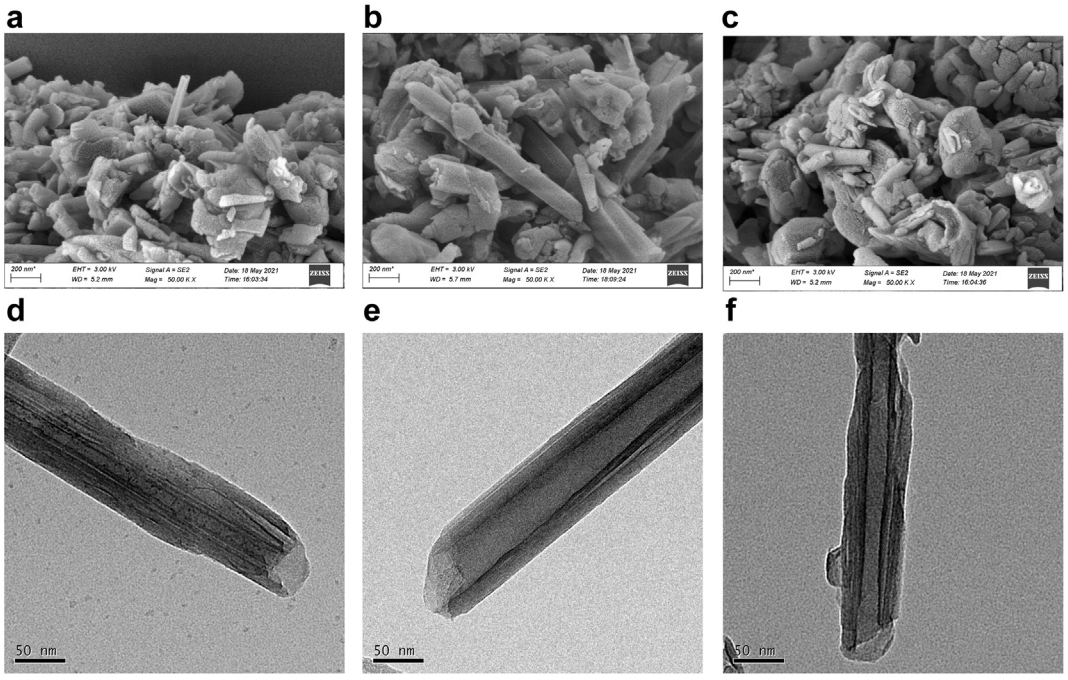

Figure 2. The scanning electron micrograph (SEM) of (a) CS, (b) CS-NHTs and (c) lac@CS-NHTs. The transmission electron microscope (TEM) of (d) CS, (e) CS-NHTs and (f) lac@CS-NHTs.

(Figure 2e) and lac@CS-HNTs (Figure 2f) were performed via a FEI TF20 transmission electron microscope. It was observed that the average length of HNT and CS-HNT was about 600 nm, the inner diameter was about 20–30 nm, and the outer diameter was about 50–70 nm. The CS-NHTs became blurred in the inner lumen and outer surface, which indicated CS was loaded on the surface of HNTs. In addition, the increase of the outer diameter of CS-HNTs confirmed the success of CS grafting on HNTs to a certain extent.

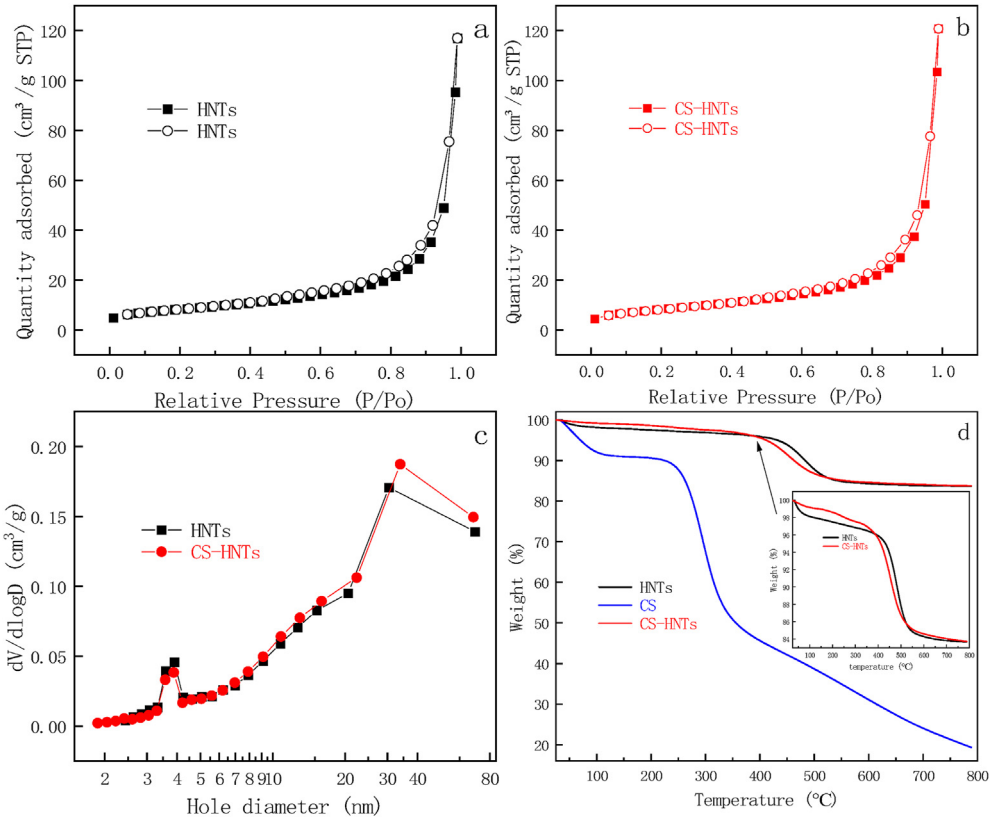

Figure 3. The N_2 adsorption-desorption curve of (a) HNTs and (b) CS-HNTs. (c) The pore size distribution of HNTs and CS-HNTs. (d) The TGA of HNTs, CS and CS-HNTs.

The surface area (Figure 3a and Figure 3b) and pore size distribution (Figure 3c) of the CS and CS-NHTs were revealed by N_2 adsorption-desorption measurements. It could be seen from Figure 3a and b that the adsorption curves and desorption curves of both HNTs and CS-HNTs are not consistent, and there were obvious hysteresis loops. The adsorption isotherms of both NHTs and CS-NHTs belong to type IV [39], indicating that HNTs and CS-HNTs were mesoporous materials. In addition, the BET surface area of the CS-HNTs was calculated to be 35.18 m^2/g, which was higher than that of HNTs (29.23 m^2/g). This is because the HNTs were modified with CS to impart amine groups to the surface. As is known to all, CS is a suitable macromolecule with abundant amino groups. Besides, as shown in Figure 3c, the average diameter of HNTs and CS-HNTs was 25 and 30 nm, respectively. The high BET surface area and the proper pore diameter were conducive to the contact with laccase molecules for catalytic reactions. Figure 3d showed the TGA analysis of HNTs, CS-HNTs and CS, the decomposition of HNTs and CS-HNTs identified two weight-loss steps below 800 °C. The first step from 100 to 400 °C was ascribed to the free/adsorbed water and interlayer water in HNTs and aluminosilicate layers, respectively. The second step from 400 to 550 °C was attributed to the dihydroxylation of the aluminosilicate lattice. Combined with the weight loss curve of CS, it could be found that the more weight loss of CS-NHTs in the second stage (400–550 °C) was due to the decomposition of the load CS. This phenomenon also reflected that CS was indeed loaded on NHTs to form CS-NHTs complexes.

XRD analysis of NHTs and CS-NHTs (Figure 4a) revealed the presence of a peak appeared at 2θ values of 12.25°, 20.01°, 24.78° and 35.01°, respectively. The corresponding crystal planes were (001), (100), (002) and (110), respectively, which confirmed the characteristics of halloysite nanotubes. In case of CS-HNTs, apart from the characteristic peaks of HNTs, there was no significant change observed in the peak pattern of HNTs. Compared with the XRD pattern of HNTs, the characteristic diffraction peak of CS-HNTs was relatively weak, which may be due to the decrease of crystallinity. After enzyme immobilization, no large changes in peak patterns were observed, from which it can be determined that enzyme immobilization did not cause further changes in the crystallinity of the nanocomposites. As shown in Figure 4b, the FTIR analysis of HNT and CS-HNTs was performed on a Thermo Scientific Nicolet 6700 fourier transform infrared spectrometer. For NHTs and CS-HNTs, the common characteristic peak of Al–OH bending was observed at 912 cm^{-1}; the common characteristic peaks of Si–O–Si and O–H stretching were observed at 1036 cm^{-1} and 3622 cm^{-1}, respectively. The above characteristic peaks were the characteristic peaks of HNTs, and the report of Rawtani et al. [40] has the same results as this study. For CS-HNTs, the new characteristic peak of C–H stretch was observed at 1633 cm^{-1}; and new characteristic peak of N–H stretch peak was observed at 3450 cm^{-1}, which showed that CS introduced new groups.

3.2. The optimal immobilization conditions on the carrier CS-HNTs

3.2.1. The effect of single factor on optimal immobilization

The preparation process of lac@CS-HNTs was optimized by controlling one-factor variables, the variables were laccase dosage (Figure 5a), pH (Figure 5b) and time (Figure 5c). The change trend of RA value and E value in Figure 5a was basically the same, both of which increase gradually and then remain stable. When the laccase dosage increased from 0.1 mg/mL to 1.0 mg/mL, the E value increased from 2.84 mg/g to 55.14 mg/g; the RA value increased from 2.84 mg/g to 55.14 mg/g which was close to the peak value. As shown in Figure 5b Evalue and RA value both increased first and then decreased. When the pH increased from 2 to 4, the E value increased from 23.10 mg/g to the maximum value (51.37 mg/g); the RA value also increased from 79.48 % to 100 %. When pH was more than 4, E value and RA value decreased rapidly. Usually, the pH of the solution affects the existence of surface charges of laccase and CS-HNTs and also affects the expression of laccase activity [41]. As shown in Figure 5c, the isoelectric point of CS-NHTs is 4.4 and the isoelectric point of FL is 3.5 according to the known report [42, 43]. When pH ranges from 3.5 to 4.4, the surface of FL was negatively charged but the surface of CS-NHTs was positively charged, the opposite surface charge would cause electrostatic attraction, which was conducive to the adsorption of FL on the CS-HNTs surface. On the contrary, when the pH range is less than 3.5 or greater than 4.4, the same surface charge will cause electrostatic repulsion, which would affect the loading performance of FL. The effect of reaction time on immobilization was similar to that of pH, E value and RA value both increased first and then decreased. When the pH increased from 0.5 to 3.0, the E value and R value increased from 9.90 mg/g and 24.66 % to the maximum value, which was due to the binding of FL to active sites on the carrier. After more than 3 h, the active sites of CS-HNTs have been fully occupied and reached saturation, RA value and E value no longer increased or even decreased slowly. The results of multiple factors affecting the immobilization conditions are described in the supplementary material (Table S1, Table S2, Table S3 and Figure S2).

3.3. The study on the enzyme stability and enzyme kinetics

3.3.1. Enzyme stability

We have evaluated the thermostability (Figure 6a), thermal tolerance (Figure 6b), pH stability (Figure 6c) and storage stability (Figure 6d) of lac@CS-NHTs. In this study, laccase was immobilized on CS-HNTs by simultaneous adsorption-covalent binding, providing a relatively lagging environment for enzyme molecules [44]. As shown in Figure 6a, the RA of the FL decreased faster with temperature relative to immobilized laccase, while the RA of lac@CS-NHTs was always greater than that of FL. This is because lac@CS-NHTs protects the tertiary structure of the enzyme protein. To further explore the thermal tolerance of lac@CS-NHTs, both the FL and lac@CS-NHTs were incubated at 50 °C for

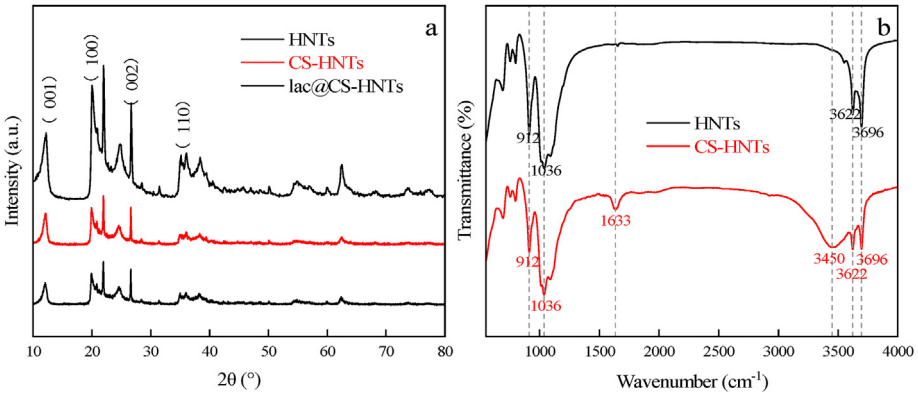

Figure 4. (a) The XRD patterns of HNTs and CS-HNTs. (b) The FTIR spectra of HNTs and CS-HNTs.

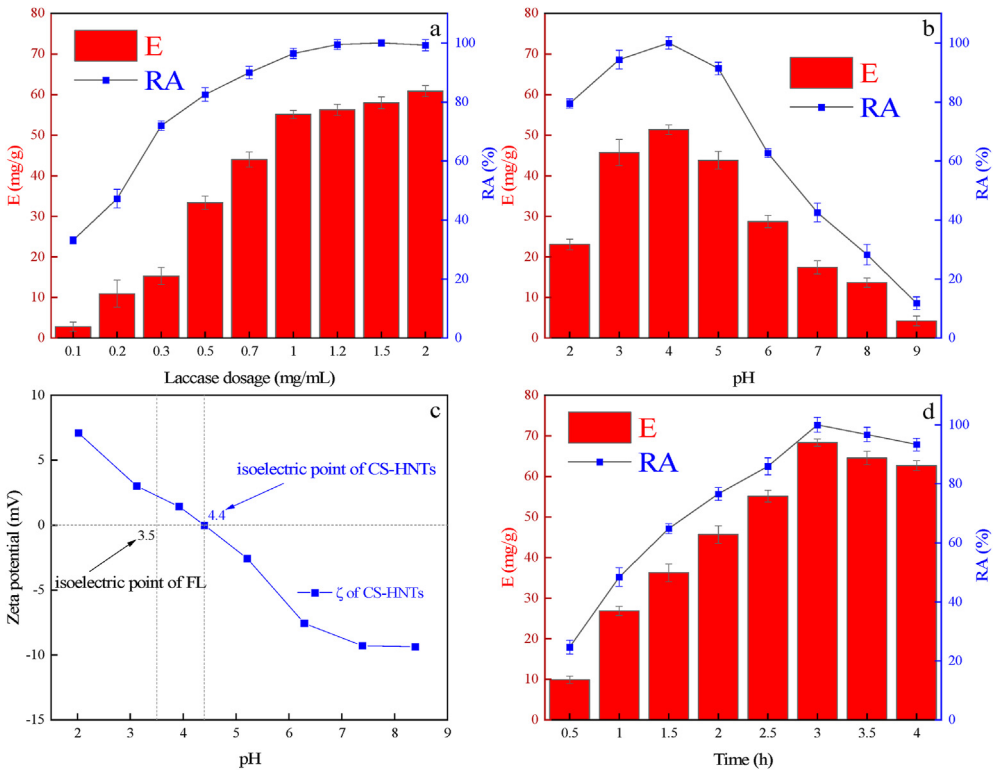

Figure 5. (a) The effect of laccase dosage on the preparation of immobilized laccase. (b) The effect of pH on the preparation of immobilized laccase. (c) Zeta potential of CS-HNTs. (d) The effect of time on the preparation of immobilized laccase.

2 h, and the RA was measured per 10 min (Figure 6b). The results showed that the RA of both FL and lac@CS-NHTs decreased with time, but the activity of immobilized laccase declined more slowly. The structure and activity of laccase are greatly affected by the pH value of the solution, because the pH value determines the ionization state of amino acids [45]. Figure 6c revealed the effect of pH on laccase, it can be seen that the

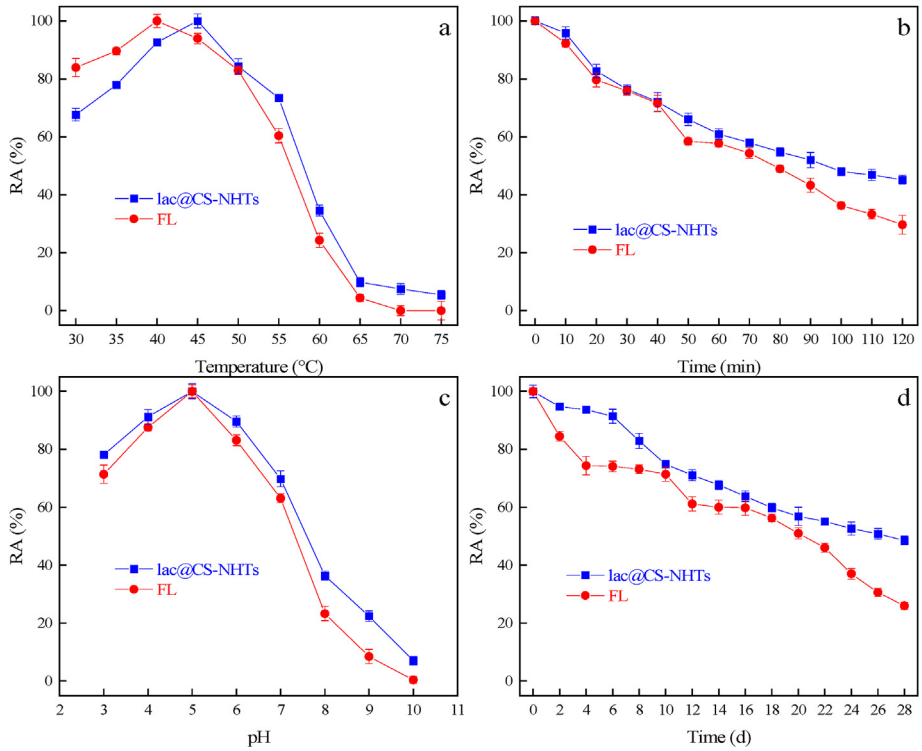

Figure 6. (a) The thermostability of FL and lac@CS-NHTs under the optimal preparation conditions. (b) The thermal tolerance of FL and lac@CS-NHTs under the optimal preparation conditions. (c) The pH stability of FL and lac@CS-NHTs under the optimal preparation conditions. (d) The storage stability of FL and lac@CS-NHTs under the optimal preparation conditions.

effect of pH on FL is stronger than that on lac@CS-NHTs, which indicates that the immobilization of laccase can broaden the tolerable pH range to a certain extent. In addition, as shown in Figure 6d, the storage stability of laccase was assessed by measuring the activities of FL and lac@CS-NHT per 2 d (storage at 4 °C for 28 d). It could be observed that after 28 d, the RA of FL was 25.60%, while the RA of lac@CS-NHTs was 48.56%. This indicated that immobilized laccase was more resistant to storage and retains more activity than free laccase [46]. As shown in Figure S4 in the supplementary material, the reusability of lac@CS-NHTs during 8 reaction cycles was investigated via BPA as substrate under the optimum reaction conditions. The results showed that the RA dropped to about 44.24 % after 8 cycles.

3.3.2. Enzyme kinetics

The reaction rate of laccase with ABTS under optimal reaction conditions was used to determine the Michaelis-Menten kinetic parameters [47] (K_m and V_{max}). The binding ability of enzyme to substrate and the speed of catalytic reaction were studied by enzyme kinetics. K_m could reflect the affinity between the laccase and BPA, and the V_{max} could reflect maximum response speed. The kinetic parameters K_m and V_{max} were calculated from the kinetic fitting curves of FL (Figure S3a in the supplementary material) and lac@CS-NHTs (Figure S3b in the supplementary material), the linear fitting equation of FL was $1/V = 28.941*1/S + 0.3795$ ($R^2 = 0.9994$); the linear fitting equation of immobilized laccase was $1/V = 246.27*1/S + 1.7315$ ($R^2 = 0.9971$). The K_m values of FL and lac @CS-NHTs could be calculated as 76.26 μM and 142.23 μM, respectively. This indicated that the affinity of FL to the substrate was higher than that of immobilized laccase, which might be due to the covalent binding of laccase on CS-HNTs resulting in loss of activity [48]. In addition, the results of Table 1 showed the enzymatic parameters of different immobilized laccase in other literatures in recent years (stability data: relative activity > 50 %), which demonstrated that the data of this work are comparable to the data in other literature. This illustrated the potential of lac@CS-NHTs in industrial applications and also provided a reference for the research of CS-NHTs in the field of immobilized laccase.

3.4. The effects of different factors on BPA removal

The batch degradation experiment of BPA was conducted by controlling one-factor variables, the variables were pH (Figure 7a), BPA initial concentration (Figure 7b), time (Figure 7c) and temperature (Figure 7d). It is worth mentioning that the heat-inactivated lac@CS-NHTs were also involved in the batch degradation experiments of BPA, which was to exclude the effect of the adsorption of BPA via lac@CS-NHTs on the results. As shown in Figure 7a, it can be seen that both FL obtained the maximum W value (79.58 %) and lac@CS-NHTs obtained the maximum R value (85.04 %) at pH 5, while the R value of inactivated lac@CS-NHTs was only 9.66 %. The acidic conditions are favorable for the catalytic reaction of laccase [52], which is consistent with the conclusion of the stability of laccase. Figure 7a showed that the adsorption effect of inactivated lac@CS-HNTs on BPA was stable in the pH range of 3–9, indicating that the binding affinity between BPA and inactivated lac@CS-HNTs was the main factor for the adsorption process. The lac@CS-HNTs reached the maximum adsorption capacity at pH 5, but the adsorption capacity decreased significantly with increasing pH. It might be because when pH < 7.6, BPA mainly exists in molecular form, while when pH > 7.6, BPA gradually dissociates into $HBPA^-$ and BPA^{2-} [53]. According to the known report, the isoelectric point of CS-NHTs is 4.4 [42], indicating that the surface of inactivated lac@CS-HNTs was negatively charged at pH > 4.4. Therefore, under alkaline conditions, the electrostatic repulsion gradually increased with the increase of pH and gradually became the main driving force. Moreover, as shown in Figure 7b, the W/R value of FL and lac@CS-NHTs both increased gradually and then remain stable. When the initial BPA concentration was 40 mg/L, the BPA degradation amount of FL was close to the maximum value of 2.63 mg and the BPA removal amount of lac@CS-NHTs was 2.75 mg. In this case, the maximum BPA adsorption removal amount of inactivated lac@CS-HNTs was 0.03 mg. Figure 7c demonstrated the effect of reaction time on BPA degradation/removal, according to the results of the enzyme kinetics study, FL has a better affinity for BPA, so the FL reached the maximum W value (88.83 %) at 10 h, while the lac@CS-HNTs reached the maximum R value (80.43 %) at 12 h. In addition, the inactivated lac@CS-NHTs reached adsorption saturation after 6 h, and the R value was only 10.14 %. As for the influence of temperature on the degradation/removal effect (Figure 7d), the curves of FL and lac@CS-NHTs both showed a mountain-like distribution. The FL reached the maximum W value (86.78 %) at 35 °C, while the lac@CS-NHTs reached the maximum R value (87.31 %) at 45 °C. This might be due to the gradual inactivation of FL as the temperature increased, but the immobilization process enhanced the thermostability and thermal tolerance of laccase. It is worth mentioning that the R value of inactivated lac@CS-NHTs increased with the increase of temperature, reaching a maximum of 30.44 % at 55 °C, which indicated that high temperature was beneficial to the adsorption of BPA via CS-NHTs.

3.5. Degradation mechanism and mineralization pathway of BPA

According to the batch removal experiment results of BPA, we found that the removal rate of inactivated lac@CS-NHTs was much lower than that of the group containing laccase, which indicated that the contribution of biodegradation was greater than adsorption. Hence, in order to further study the degradation mechanism and mineralization pathway of BPA by lac@CS-HNTs, the high-performance liquid chromatography (HPLC, UltiMate 3000, DIONEX) and Agilent 7890B gas chromatography-mass (GC-MS) spectrometer (USA) was used to

Table 1. The comparison of enzymatic parameters of different immobilized laccases (stability data: relative activity > 50 %).

Carrier	Chitosan	Polyvinylidene fluoride nanocomposite	Metal organic framework	Magnetic biochar	Chitosan functionalized halloysite nanotubes	Free laccase
Year	2021	2021	2019	2020	2022	2022
Source	*Pleurotus nebrodensis*	*Trametes hirsuta*	*white rot fungi*	*Trametes versicolor*	*Trametes versicolor*	*Trametes versicolor*
Method	Adsorption-crosslinking	Adsorption	Covalent binding	Adsorption	Adsorption-crosslinking	–
Enzyme loading	–	30.40 mg/cm^2	69.11 mg/g	27.00 mg/g	68.33 mg/g	–
K_m (μM)	120	–	771		142.23	76.26
pH stability	6–10	–	2–7	4–8	3–7.5	3–7
Storage stability	–	–	>28 d	>30 d	>28 d	<20 d
Reusability	8	2	2	7	7	–
Thermostability	25–70 °C	25–70 °C	25–65 °C	25–55 °C	25–55 °C	25–50 °C
Reference	[49]	[50]	[48]	[51]	This work	This work

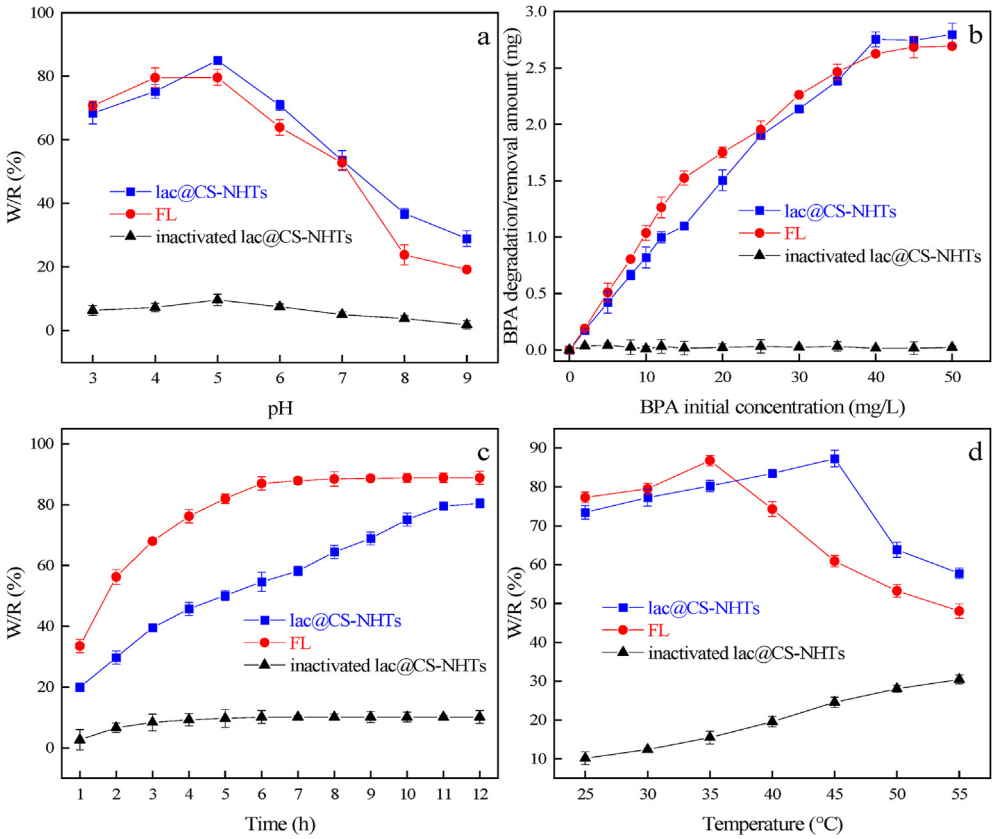

Figure 7. (a) The effects of pH on BPA removal. (b) The effects of BPA initial concentration on BPA removal. (c) The effects of time on BPA removal. (d) The effects of temperature on BPA removal.

detect the degradation products of BPA (Figure S5 in supplementary material). Table S4 in supplementary material showed the intermediate products identified at samples (0–12 h) form during the BPA degradation and mineralization. Compared with the standard library, it was found that the intermediate products of BPA degradation might contain 4-isopropenylphenol, 2,4-Bis(2-methyl-2-propanyl)phenol, 4,4′-prop-1-ene-1,2-diyldiphenol, 2,2′-methylenebis(6-tert-butyl-4-methylphenol), etc. The existing studies on BPA degradation pathways are similar to our reports [54, 55, 56, 57]. Liu et al. [21] studied the interaction between free laccase and BPA via molecular docking simulation. They found that the reaction between laccase and BPA was spontaneous via the docking results. It is worth mentioning that they found BPA degradation by free laccase started from the C atoms between two benzene rings.

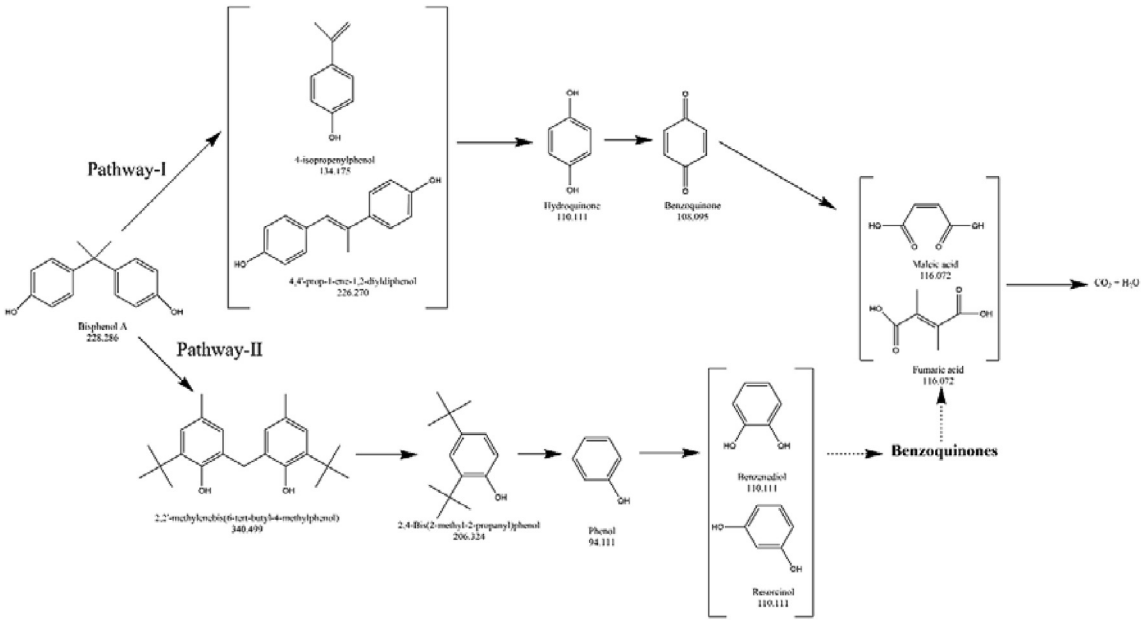

Figure 8. The possible pathways during the BPA degradation and mineralization via lac@CS-NHTs in aqueous solution.

Therefore, combined with the spectra and related reports [58, 59], we speculated that the mineralization pathway of BPA via lac@CS-NHTs are as shown in Figure 8. In the pathway-I, BPA was attacked by laccase-generated ·OH with the formation of 4,4′-prop-1-ene-1,2-diyldiphenol and 4-isopropenylphenol, which were oxidized to form hydroquinone and further transform into 1,4-benzoquinone. In the pathway-II, degradation of BPA yields 2,2′-methylenebis(6-tert-butyl-4-methylphenol) that further transformed as 2,4-Bis(2-methyl-2-propanyl)phenol via oxidative skeletal rearrangement. Next, 2,4-Bis(2-methyl-2-propanyl) phenol was transformed into phenol and further transformed into catechol or resorcinol via laccase. Similar to pathway-I, both catechol and resorcinol were further converted to corresponding benzoquinones [60, 61, 62, 63]. Finally, according to a large number of reported literatures [64, 65, 66, 67], benzoquinones were oxidized to small molecular organic acids such as maleic acid and fumaric acid, and eventually mineralized to H_2O and CO_2.

4. Conclusion

In conclusion, laccase was immobilized on CS-HNTs by simultaneous adsorption-covalent binding method to remove BPA for the first time. Under the optimal preparation conditions, lac@CS-NHTs obtained the maximum enzyme activity, and the enzyme loading was as high as 60.10 mg/g. The results of batch removal experiment of BPA showed that under the optimum treatment condition (pH 5, BPA 40 mg/L, 12 h, 45 °C), the BPA removal rate of lac@CS-NHTs, FL and heat-inactivated lac@CS-NHTs was 87.31 %, 60.89 % and 24.54 %, respectively, which indicated that the contribution of biodegradation was greater than adsorption. In addition, the relative activity of lac@CS-NHTs dropped to about 44.24 % after 8 cycles of BPA removal, which demonstrated that lac@CS-NHTs have the potential to reduce costs in practical applications. Finally, the possible degradation mechanism showed that the BPA degradation mainly depends on the hydroxyl radical formation via laccase. The mineralization pathways were proposed based on the intermediate byproducts identify by GC-MS and HPLC analysis at the optimum treatment condition.

Declarations

Author contribution statement

Zhaobo Wang: Conceived and designed the experiments; Performed the experiments; Analyzed and interpreted the data; Contributed reagents, materials, analysis tools or data; Wrote the paper.

Dajun Ren, Xiaoqing Zhang, Shuqin Zhang, Wangsheng Chen: Analyzed and interpreted the data; Contributed reagents, materials, analysis tools or data.

Yaohui Cheng: Performed the experiments; Analyzed and interpreted the data; Wrote the paper.

Funding statement

This work was supported by Science and Technology Innovation Team Project of Hubei Provincial Department of Education (T2020002), Wuhan Science and Technology Planning Project (2020020601012274), National Natural Science Foundation of China (41571306) and Hubei Technological Innovation Special Fund (2020ZYYD019).

Data availability statement

Data included in article/supplementary material/referenced in article.

Declaration of interests statement

The authors declare no conflict of interest.

Additional information

Supplementary content related to this article has been published online at https://doi.org/10.1016/j.heliyon.2022.e09919.

Acknowledgements

The authors would like to thank Jiang Lang from Shiyanjia Lab (www.shiyanjia.com) for the characterization support.

References

[1] S. Sifakis, V.P. Androutsopoulos, A.M. Tsatsakis, D.A. Spandidos, Human exposure to endocrine disrupting chemicals: effects on the male and female reproductive systems, Environ. Toxicol. Pharmacol. 51 (2017) 56–70.
[2] Y.Z. Lv, L. Yao, L. Wang, W.R. Liu, J.L. Zhao, L.Y. He, G.G. Ying, Bioaccumulation, metabolism, and risk assessment of phenolic endocrine disrupting chemicals in specific tissues of wild fish, Chemosphere 226 (2019) 607–615.
[3] A. Mantovani, Endocrine disrupters and the safety of food chains, Horm. Res. Paediatr. 86 (2016) 279–288.
[4] P. Alonso-Magdalena, A.B. Ropero, S. Soriano, M. García-Arévalo, C. Ripoll, E. Fuentes, I. Quesada, Á. Nadal, Bisphenol-A acts as a potent estrogen via non-classical estrogen triggered pathways, Mol. Cell. Endocrinol. 355 (2012) 201–207.
[5] A. Careghini, A.F. Mastorgio, S. Saponaro, E. Sezenna, Bisphenol A, nonylphenols, benzophenones, and benzotriazoles in soils, groundwater, surface water, sediments, and food: a review, Environ. Sci. Pollut. Res. Int. 22 (2015) 5711–5741.
[6] A. Marqueno, E. Perez-Albaladejo, C. Flores, E. Moyano, C. Porte, Toxic effects of bisphenol A diglycidyl ether and derivatives in human placental cells, Environ. Pollut. 244 (2019) 513–521.
[7] C. Xiao, L. Wang, Q. Zhou, X. Huang, Hazards of bisphenol A (BPA) exposure: a systematic review of plant toxicology studies, J. Hazard Mater. 384 (2020), 121488.
[8] A. Bhatnagar, I. Anastopoulos, Adsorptive removal of bisphenol A (BPA) from aqueous solution: a review, Chemosphere 168 (2017) 885–902.
[9] M. Umar, F. Roddick, L. Fan, H.A. Aziz, Application of ozone for the removal of bisphenol A from water and wastewater–a review, Chemosphere 90 (2013) 2197–2207.
[10] M. Bilal, H.M.N. Iqbal, D. Barceló, Mitigation of bisphenol A using an array of laccase-based robust bio-catalytic cues–a review, Sci. Total Environ. 689 (2019) 160–177.
[11] Z. Li, F. Wang, Y. Zhang, Y. Lai, Q. Fang, Y. Duan, Activation of peroxymonosulfate by CuFe2O4-CoFe2O4 composite catalyst for efficient bisphenol a degradation: synthesis, catalytic mechanism and products toxicity assessment, Chem. Eng. J. 423 (2021).
[12] Y.M. Hunge, A.A. Yadav, S. Khan, K. Takagi, N. Suzuki, K. Teshima, C. Terashima, A. Fujishima, Photocatalytic degradation of bisphenol A using titanium dioxide@nanodiamond composites under UV light illumination, J. Colloid Interface Sci. 582 (2021) 1058–1066.
[13] G. Kyrila, A. Katsoulas, V. Schoretsaniti, A. Rigopoulos, E. Rizou, S. Doulgeridou, V. Sarli, V. Samanidou, M. Touraki, Bisphenol A removal and degradation pathways in microorganisms with probiotic properties, J. Hazard Mater. 413 (2021), 125363.
[14] F. Gassara, S.K. Brar, M. Verma, R.D. Tyagi, Bisphenol A degradation in water by ligninolytic enzymes, Chemosphere 92 (2013) 1356–1360.
[15] L. Zhang, J. Mi, G. Hu, C. Zhang, H. Qi, Facile fabrication of a high-efficient and biocompatibility biocatalyst for bisphenol A removal, Int. J. Biol. Macromol. 150 (2020) 948–954.
[16] C. Nicolucci, S. Rossi, C. Menale, T. Godjevargova, Y. Ivanov, M. Bianco, L. Mita, U. Bencivenga, D.G. Mita, N. Diano, Biodegradation of bisphenols with immobilized laccase or tyrosinase on polyacrylonitrile beads, Biodegradation 22 (2011) 673–683.
[17] A. Grelska, M. Noszczyńska, White rot fungi can be a promising tool for removal of bisphenol A, bisphenol S, and nonylphenol from wastewater, Environ. Sci. Pollut. Control Ser. (2020) 1–19.
[18] Ming Chen, Guangming Zeng, Lai Cui, Chang Zhang, Piao Xu, Min Yan, W. Xiong, Interactions of carbon nanotubes and/or graphene with manganese peroxidase during biodegradation of endocrine disruptors and triclosan, Chemosphere 184 (2017) 127–136.
[19] W. Zhou, W. Zhang, Y. Cai, Laccase immobilization for water purification: a comprehensive review, Chem Eng J 403 (2021), 126272.
[20] A.I. Cañas, S. Camarero, Laccases and their natural mediators: biotechnological tools for sustainable eco-friendly processes, Biotechnol. Adv. 28 (2010) 694–705.
[21] L. Hongyan, Z. Zexiong, X. Shiwei, X. He, Z. Yinian, L. Haiyun, Y. Zhongsheng, Study on transformation and degradation of bisphenol A by Trametes versicolor laccase and simulation of molecular docking, Chemosphere 224 (2019) 743–750.
[22] N.A. Daronch, M. Kelbert, C.S. Pereira, P.H.H. de Araújo, D. de Oliveira, Elucidating the choice for a precise matrix for laccase immobilization: a review, Chem. Eng. J. 397 (2020), 125506.
[23] D. Ren, Z. Wang, S. Jiang, H. Yu, S. Zhang, X. Zhang, Recent environmental applications of and development prospects for immobilized laccase: a review, Biotechnol. Genet. Eng. Rev. 36 (2020) 81–131.
[24] C. Mateo, J.M. Palomo, G. Fernandez-Lorente, J.M. Guisan, R. Fernandez-Lafuente, Improvement of enzyme activity, stability and selectivity via immobilization techniques, Enzym. Microb. Technol. 40 (2007) 1451–1463.

[25] G. Yaohua, X. Ping, J. Feng, S. Keren, Co-immobilization of laccase and ABTS onto novel dual-functionalized cellulose beads for highly improved biodegradation of indole, J. Hazard Mater. 365 (2019) 118–124.
[26] Z. Wang, D. Ren, H. Yu, S. Zhang, X. Zhang, W. Chen, Preparation optimization and stability comparison study of alkali-modified biochar immobilized laccase under multi-immobilization methods, Biochem. Eng. J. 181 (2022), 108401.
[27] B. Yang, K. Tang, S. Wei, X. Zhai, N. Nie, Preparation of functionalized mesoporous silica as a novel carrier and immobilization of laccase, Appl. Biochem. Biotechnol. (2021) 1–20.
[28] Z. Wang, D. Ren, J. Wu, S. Jiang, H. Yu, Y. Cheng, S. Zhang, X. Zhang, Study on adsorption-degradation of 2, 4-dichlorophenol by modified biochar immobilized laccase, Int. J. Environ. Sci. Technol. (2021) 1–14.
[29] X. Qiu, S. Wang, S. Miao, H. Suo, H. Xu, Y. Hu, Co-immobilization of laccase and ABTS onto amino-functionalized ionic liquid-modified magnetic chitosan nanoparticles for pollutants removal, J. Hazard Mater. 401 (2021), 123353.
[30] A.A. Kadam, B. Sharma, S.K. Shinde, G.S. Ghodake, G.D. Saratale, R.G. Saratale, D.-Y. Kim, J.-S. Sung, Thiolation of chitosan loaded over super-magnetic halloysite nanotubes for enhanced laccase immobilization, Nanomaterials 10 (2020) 2560.
[31] A.A. Kadam, J. Jang, S.C. Jee, J.-S. Sung, D.S. Lee, Chitosan-functionalized supermagnetic halloysite nanotubes for covalent laccase immobilization, Carbohydr. Polym. 194 (2018) 208–216.
[32] M. Kim, S.C. Jee, J.-S. Sung, A.A. Kadam, Anti-proliferative applications of laccase immobilized on super-magnetic chitosan-functionalized halloysite nanotubes, Int. J. Biol. Macromol. 118 (2018) 228–237.
[33] R. Hürmüzlü, M. Okur, N. Saraçoğlu, Immobilization of Trametes versicolor laccase on chitosan/halloysite as a biocatalyst in the Remazol Red RR dye, Int. J. Biol. Macromol. 192 (2021) 331–341.
[34] M. Tharmavaram, G. Pandey, P. Bhatt, P. Prajapati, D. Rawtani, K.P. Sooraj, M. Ranjan, Chitosan functionalized Halloysite Nanotubes as a receptive surface for laccase and copper to perform degradation of chlorpyrifos in aqueous environment, Int. J. Biol. Macromol. 191 (2021) 1046–1055.
[35] C. Jiang, G. Sun, Z. Zhou, Z. Bao, X. Lang, J. Pang, Q. Sun, Y. Li, X. Zhang, C. Feng, X. Chen, Optimization of the preparation conditions of thermo-sensitive chitosan hydrogel in heterogeneous reaction using response surface methodology, Int. J. Biol. Macromol. 121 (2019) 293–300.
[36] S.-N. Nam, H. Cho, J. Han, N. Her, J. Yoon, Photocatalytic degradation of acesulfame K: optimization using the Box–Behnken design (BBD), Process Saf. Environ. Protect. 113 (2018) 10–21.
[37] R. Bourbonnais, D. Leech, M.G. Paice, Electrochemical analysis of the interactions of laccase mediators with lignin model compounds, Biochim. Biophys. Acta Gen. Subj. 1379 (1998) 381–390.
[38] F. Wang, C. Guo, L.R. Yang, C.Z. Liu, Magnetic mesoporous silica nanoparticles: fabrication and their laccase immobilization performance, Bioresour. Technol. 101 (2010) 8931–8935.
[39] K. Kaneko, H. Otsuka, New IUPAC recommendation and characterization of nanoporous materials with physical adsorption vol. 5, 2020, pp. 25–32.
[40] D. Rawtani, G. Pandey, M. Tharmavaram, P. Pathak, S. Akkireddy, Y.K. Agrawal, Development of a novel 'nanocarrier' system based on Halloysite Nanotubes to overcome the complexation of ciprofloxacin with iron: an in vitro approach, Appl. Clay Sci. 150 (2017) 293–302.
[41] V. Van Tran, D. Park, Y.-C. Lee, Hydrogel applications for adsorption of contaminants in water and wastewater treatment, Environ. Sci. Pollut. Control Ser. 25 (2018) 24569–24599.
[42] H. Lun, J. Ouyang, H. Yang, Enhancing dispersion of halloysite nanotubes via chemical modification, Phys. Chem. Miner. 41 (2014) 281–288.
[43] M. Zhang, F. Wu, Z.Y. Wei, Y.Z. Xiao, W.M. Gong, Characterization and decolorization ability of a laccase from Panus rudis, Enzym. Microb. Technol. 39 (2006) 92–97.
[44] A.I. El-Batal, N.M. ElKenawy, A.S. Yassin, M.A. Amin, Laccase production by Pleurotus ostreatus and its application in synthesis of gold nanoparticles, Biotechnol. Rep. 5 (2015) 31–39.
[45] M. Taheran, M. Naghdi, S.K. Brar, E.J. Knystautas, M. Verma, R.Y. Surampalli, Degradation of chlortetracycline using immobilized laccase on Polyacrylonitrile-biochar composite nanofibrous membrane, Sci. Total Environ. 605 (2017) 315–321.
[46] J. Zdarta, K. Antecka, R. Frankowski, A. Zgoła-Grześkowiak, H. Ehrlich, T. Jesionowski, The effect of operational parameters on the biodegradation of bisphenols by Trametes versicolor laccase immobilized on Hippospongia communis spongin scaffolds, Sci. Total Environ. 615 (2018) 784–795.
[47] M. Kelbert, C.S. Pereira, N.A. Daronch, K. Cesca, C. Michels, D. de Oliveira, H.M. Soares, Laccase as an efficacious approach to remove anticancer drugs: a study of doxorubicin degradation, kinetic parameters, and toxicity assessment, J. Hazard Mater. 409 (2021), 124520.
[48] E. Wu, Y. Li, Q. Huang, Z. Yang, A. Wei, Q. Hu, Laccase immobilization on amino-functionalized magnetic metal organic framework for phenolic compound removal, Chemosphere 233 (2019) 327–335.
[49] S. Aslam, M. Asgher, N.A. Khan, M. Bilal, Immobilization of Pleurotus nebrodensis WC 850 laccase on glutaraldehyde cross-linked chitosan beads for enhanced biocatalytic degradation of textile dyes, J. Water Proc. Eng. 40 (2021), 101971.
[50] M. Masjoudi, M. Golgoli, Z.G. Nejad, S. Sadeghzadeh, S.M. Borghei, Pharmaceuticals removal by immobilized laccase on polyvinylidene fluoride nanocomposite with multi-walled carbon nanotubes, Chemosphere 263 (2021), 128043.
[51] Y. Zhang, M. Piao, L. He, L. Yao, T. Piao, Z. Liu, Y. Piao, Immobilization of laccase on magnetically separable biochar for highly efficient removal of bisphenol A in water, RSC Adv. 10 (2020) 4795–4804.
[52] M.L. Toledo, M.M. Pereira, M.G. Freire, J.P.A. Silva, J.A.P. Coutinho, A.P.M. Tavares, Laccase activation in deep eutectic solvents, Acs Sustain. Chem. Eng. 7 (2019) 11806–11814.
[53] D. Bing-zhi, C. Hua-qiang, W. Lin, X. Sheng-ji, G. Nai-yun, The removal of bisphenol A by hollow fiber microfiltration membrane, Desalination 250 (2010) 693–697.
[54] T. Taghizadeh, A. Talebian-Kiakalaieh, H. Jahandar, M. Amin, S. Tarighi, M.A. Faramarzi, Biodegradation of bisphenol A by the immobilized laccase on some synthesized and modified forms of zeolite Y, J. Hazard Mater. 386 (2020), 121950.
[55] J. Liu, F. Xie, R. Li, T. Li, Z. Jia, Y. Wang, Y. Wang, X. Zhang, C. Fan, TiO2-x/Ag3PO4 photocatalyst: oxygen vacancy dependent visible light photocatalytic performance and BPA degradative pathway, Mater. Sci. Semicond. Process. 97 (2019) 1–10.
[56] C.F. Zorzo, J.J. Inticher, F.H. Borba, L.C. Cabrera, J.S. Dugatto, S. Baroni, G.K. Kreutz, D. Seibert, R. Bergamasco, Oxidative degradation and mineralization of the endocrine disrupting chemical bisphenol-A by an eco-friendly system based on UV-solar/H2O2 with reduction of genotoxicity and cytotoxicity levels, Sci. Total Environ. 770 (2021), 145296.
[57] G. Kyrila, A. Katsoulas, V. Schoretsaniti, A. Rigopoulos, E. Rizou, S. Doulgeridou, V. Sarli, V. Samanidou, M. Touraki, Bisphenol A removal and degradation pathways in microorganisms with probiotic properties, J. Hazard Mater. 413 (2021), 125363.
[58] R. Das, Z. Liang, G. Li, B. Mai, T. An, Genome sequence of a spore-laccase forming, BPA-degrading Bacillus sp. GZB isolated from an electronic-waste recycling site reveals insights into BPA degradation pathways, Arch. Microbiol. 201 (2019) 623–638.
[59] Y. Yuan, W. Cai, J. Xu, J. Cheng, K.-S. Du, Recyclable laccase by coprecipitation with aciduric Cu-based MOFs for bisphenol A degradation in an aqueous environment, Colloids Surf. B Biointerfaces 204 (2021), 111792.
[60] D. Daàssi, A. Prieto, H. Zouari-Mechichi, M.J. Martínez, M. Nasri, T. Mechichi, Degradation of bisphenol A by different fungal laccases and identification of its degradation products, Int. Biodeterior. Biodegrad. 110 (2016) 181–188.
[61] R. Das, G. Li, B. Mai, T. An, Spore cells from BPA degrading bacteria Bacillus sp. GZB displaying high laccase activity and stability for BPA degradation, Sci. Total Environ. 640–641 (2018) 798–806.
[62] J. Sharma, I.M. Mishra, D.D. Dionysiou, V. Kumar, Oxidative removal of Bisphenol A by UV-C/peroxymonosulfate (PMS): kinetics, influence of co-existing chemicals and degradation pathway, Chem. Eng. J. 276 (2015) 193–204.
[63] B. Kolvenbach, N. Schlaich, Z. Raoui, J. Prell, S. Zühlke, A. Schäffer, F.P. Guengerich, P.F.X. Corvini, Degradation Pathway of Bisphenol A: does ipso Substitution Apply to Phenols Containing a Quaternary α-Carbon Structure in the para Position? Appl. Environ. Microbiol. 73 (2007) 4776–4784.
[64] Z. Wu, M. Zhou, Partial degradation of phenol by advanced electrochemical oxidation process, Environ. Sci. Technol. 35 (2001) 2698–2703.
[65] A. Santos, P. Yustos, A. Quintanilla, S. Rodrıguez, F. Garcıa-Ochoa, Route of the catalytic oxidation of phenol in aqueous phase, Appl. Catal. B Environ. 39 (2002) 97–113.
[66] S. Xie, M. Li, Y. Liao, Q. Qin, S. Sun, Y. Tan, In-situ preparation of biochar-loaded particle electrode and its application in the electrochemical degradation of 4-chlorophenol in wastewater, Chemosphere 273 (2021), 128506.
[67] B. Liu, T. Pan, J. Liu, L. Feng, Y. Chen, H. Zheng, Taping into the super power and magic appeal of ultrasound coupled with EDTA on degradation of 2, 4, 6-TCP by Fe0 based advanced oxidation processes, Chemosphere 288 (2022), 132650.